Electronic Structures of MoF 6 and MoOF 4 in the Ground and Excited States: A SAC-CI and Frozen-Orbital-Analysis Study

4 AUTHORS, INCLUDING:

Hiromi Nakai
Waseda University
221 PUBLICATIONS 3,218 CITATIONS

SEE PROFILE

Pasquale Tomasello
University of Catania
24 PUBLICATIONS 246 CITATIONS

SEE PROFILE

Electronic Structures of MoF$_6$ and MoOF$_4$ in the Ground and Excited States: A SAC-CI and Frozen-Orbital-Analysis Study

Hiromi Nakai,[*,†] **Hiroshi Morita,**[‡] **Pasquale Tomasello,**[§] **and Hiroshi Nakatsuji**[‡,‖]

Department of Chemistry, School of Science and Engineering, Waseda University, Shinjuku-ku, Tokyo 169-0072, Japan, Department of Synthetic Chemistry and Biological Chemistry, Faculty of Engineering, Kyoto University, Sakyo-ku, Kyoto 606-8317, Japan, Dipartimento di Fisica, INFM and INFN Università di Catania, 57 Corso Italia, I-95129 Catania, Italy, and Institute for Fundamental Chemistry, 34-4, Takano-Nishihiraki-cho, Sakyo-ku, Kyoto 606-8103, Japan

The symmetry-adapted-cluster (SAC) and SAC-configuration interaction (SAC-CI) many-body theories have been applied to calculate, within the all-electron ab initio Hamiltonian, the singlet ground and excited states of MoF$_6$ and MoOF$_4$. Chemical bonding and electron correlation are quite important to reduce the formal charge of electrostatic Mo−ligand bonds in both ground and excited states. The calculated excited states are all characterized as electron-transfer excitations from ligands to molybdenum, reducing the ionicity of the Mo−F bonds. For MoF$_6$, we assign the energetically lower three peaks to dipole-allowed electronic transitions to the $^1T_{1u}$ excited states, consistently with the calculated oscillator strengths, and at variance of the previously proposed assignments. The fourth and fifth peaks, having very weak intensity, have been tentatively assigned to the dipole-forbidden 2^1E_g and 4^1T_{2g} excited states, respectively. The experimental excitation energies and intensities are well reproduced by the present calculations. The maximum discrepancy (0.35 eV) of the calculated excitation energies occurs for the first peak. Chemical bondings of MoOF$_4$ in the ground and excited states, although exhibiting great reductions of the ionicity, are more ionic than those of MoF$_6$. For the visible−UV spectrum of MoOF$_4$, we assign the two experimental peaks to dipole-allowed transitions to the ^1E excited states. The present assignments of the observed electronic transitions based on the accurate SAC-CI calculations should be more reliable than the previous ones. We further used the frozen-orbital-analysis (FZOA) method in order to understand and rationalize the energy orderings and splittings for the excited states having the same excitation nature. We confirm that the FZOA method is very simple and useful to examine and explain the origin of the orderings of the excitation levels. Some relationships on the orderings and splittings presented here should be of general applicability to any systems.

I. Introduction

Octahedral molybdenum hexafluoride MoF$_6$, one of the most effective fluorinating and oxidizing agents, has an extraordinary high (5−7 eV) electron affinity (EA). The valence ionization potentials (IPs) have been investigated by photoelectron spectroscopy (PES)[1] and subsequent theoretical studies within the X$_\alpha$-type methods.[2,3] Ordering and assignment of the PES peaks have been understood on the qualitative level.[2,3] We have recently shown that within the all-electron ab-initio Hamiltonian, electron-correlation effects are quite important even for a qualitative description of the valence ionized states of MoF$_6$.[4] The electron correlation was also shown to be extremely important for calculating the EA.[5]

The electronic structures of MoF$_6$ in the excited states have been early investigated by visible−UV absorption spectroscopy[6] and thereafter by semiempirical X$_\alpha$-based methods.[2,5] For the experimentally observed five bands of MoF$_6$, ranging from 6 to 11 eV, two different assignments have been proposed. Both assignments, which are based on ligand-field theory[6] and on semiempirical MO method,[2] leave room for criticism and questions.

MoOF$_4$ is obtained by oxidation of MoF$_6$ using MoO$_3$. This molecule also possesses a high EA. In its crystalline state, the MoOF$_4$ molecule forms a chain structure[7] that has not been noticed for MoF$_6$. The excited states have been investigated by visible−UV absorption spectroscopy and the X$_\alpha$ calculations.[8] Other theoretical studies on MoOF$_4$ by Sosa et al.,[9] by Neuhause et al.,[10] and by Benson et al.[11] have mainly focused on the ground state using the density functional, MP2, and SCF methods, respectively. However, similar to MoF$_6$, there have so far been no ab initio theoretical studies on the excited states of MoOF$_4$.

In the present investigation, we have calculated both excitation energies and oscillator strengths for the singlet excited states of MoF$_6$ and MoOF$_4$ by the symmetry-adapted-cluster (SAC) and SAC-configuration interaction (SAC-CI)[12,13] methods, of which the accuracy and reliability have been tested by numerous applications to diverse organic and inorganic systems (for a recent review, see ref 14). We have tried to perform assignments of the experimentally observed electronic peaks for MoF$_6$ and MoOF$_4$ by using the SAC-CI results of both calculated excitation energies and corresponding oscillator strengths.

Since MoF$_6$ has a high symmetry (O_h), most of the excited states are dipole-forbidden. It is therefore difficult to observe all the excited states of MoF$_6$ by the usual one-photon

---

[†] Waseda University.
[‡] Kyoto University.
[§] INFM and INFN Universita di Catania.
[‖] Institute for Fundamental Chemistry.

experiment. Assignments, moreover, are not easy because of the very weak intensities and partially overlapping bands. The present SAC-CI calculations have yielded both allowed and forbidden excited states up to about 11 eV, which are further analyzed in order to clarify and understand the origin of the energy ordering and splitting. In a recent paper,[15] we have proposed a frozen-orbital-analysis (FZOA) method to this end. Therein, we have applied it only to the $t_{1u} \rightarrow t_{2g}$ excited states of MoF$_6$ to show its predictive capabilities. Here, the FZOA method is applied systematically to all valence excitations of MoF$_6$. We also examine, within this method, the valence e $\rightarrow$ e excitation of MoOF$_4$. The FZOA method appears to be useful for understanding the chemical and physical meanings of the excitation levels.

In section II, we give technical details of SCF and SAC/ SAC-CI calculations for MoF$_6$ and MoOF$_4$. The used geometries, basis sets, MO active space, and some principal features of the SAC-CI theory are briefly addressed. Section III deals with results and discussions of the ground-state electronic structures and of the excitation energies for MoF$_6$ (subsections A and B) and for MoOF$_4$ (subsections C and D). In section IV, we give concluding remarks and a summary of the present work.

II. Computational Details

Geometries of MoF$_6$ and MoOF$_4$ are held at their regular octahedron and square-pyramidal configurations, respectively. Experimental data are used for bond and angle parameters. In MoF$_6$, the Mo–F bond length is set to 1.82 Å.[16] In MoOF$_4$, the Mo–F and Mo–O bond lengths are set to 1.836 and 1.650 Å, respectively.[17] The O–Mo–F and F–Mo–F angles are set to 103.8° and 86.7°, respectively.[16,17]

The Gaussian basis set used for the Mo atom is the (16s10p7d)/[6s4p3d] set of Huzinaga[18] augmented with two p (ζ_p = 0.081, 0.026) functions[18] to represent the 5p orbital and two s (ζ_s = 0.012 01, 0.005 856) and two p (ζ_p = 0.011 04, 0.005 455) Rydberg functions.[19] For fluorine, we use the (10s7p)/[3s2p] set of Huzinaga[18] augmented with two d (ζ_d = 3.559, 0.682) polarization functions[18] and one s (ζ_s = 0.036) and two p (ζ_p = 0.074, 0.0029) Rydberg functions.[20] For oxygen, we use the (9s5p)/[4s2p] set of Huzinage–Dunning[21] augmented with two d (ζ_d = 2.704, 0.535) polarization functions,[18] one s (ζ_s = 0.059) and one p (ζ_p = 0.059) diffuse functions.[20]

The all-electron SCF wave function for the ground state is calculated by using the program system HONDO8.[22] Electron correlations in the singlet ground and excited states are taken into account by the SAC/SAC-CI theory.[12,13] The active spaces in the SAC-CI calculations involve the 18 and 15 higher-energy occupied molecular orbitals (MOs) and the 127 and 109 lower-energy unoccupied MOs of MoF$_6$ and MoOF$_4$, respectively. The 43 and 36 higher-energy virtual MOs of MoF$_6$ and MoOF$_4$, respectively, are neglected. The active occupied orbitals are mainly composed of the 4d atomic orbitals (AOs) of Mo and the 2p AOs of F or O.

In the SAC-CI calculations, all single-excitation (SE) operators have been included in the linked terms. Double-excitation operators, selected by the second-order perturbation, are added in the configuration spaces. The double-excitation operators, whose perturbation energies are larger than 3×10^{-5} au, have been included for the ground-state calculations. After selection, the dimensions of the single- and double-excitation operators result in 7314 and 6177 for MoF$_6$ and MoOF$_4$, respectively. For the excited-state calculations, which have been carried out

within the D_{2h} (MoF$_6$) and C_{2v} (MoOF$_4$) subsets of O_h and C_{4v} symmetries, respectively, the energy threshold for the configuration selection is slightly modified to 4×10^{-5} au with respect to the main configurations ($C \geq 0.1$) of the 14 and 15 lower SE-CI solutions for each irreducible representation. The dimensions for the excited states are from 14 715 to 27 248. In SAC theory,[23] the effect of the simultaneous binary electron scattering (four-body collisions) is dealt with in the form of the so-called unlinked term. We include, in the unlinked term, all double-excitation operators whose coefficients in the single and double (SD) CI are larger than 1×10^{-2}. In SAC-CI theory,[2,3] it takes into account the transferable part of the electron correlation between the ground and excited states. All the SAC-CI calculations discussed in the present work have been carried out by using the standard SAC-85 program system.[24]

III. Results and Discussions

A. SAC-CI Calculations of MoF$_6$: Ground and Excited States. All valence occupied MOs of MoF$_6$ have dominant characters of ligand. In this respect, MoF$_6$ may be termed a d^0 complex. Occupied 7e$_g$, 7a$_{1g}$, and 7t$_{1u}$ MOs have σ character, whereas 2t$_{2g}$, 6t$_{1u}$, 1t$_{2u}$, and 2t$_{1g}$ MOs have π character. Unoccupied 3t$_{2g}$ (π) and 9e$_g$ (σ) MOs are Mo–F antibonding and dominantly composed of the 4d AOs of Mo.

A formal charge of +6, according to simple electrostatic ligand-field theory, should be attributed to Mo in MoF$_6$. However, the Mo–F bond actually has a large covalent character owing to the back-donation from ligand to Mo. The net charge of Mo is indeed calculated to be +1.538 at the SCF level. The ionicity of the Mo–F bond is further relaxed by inclusion of the electron correlation, resulting in +1.227 by the SAC method. An analogous situation is found in the singlet excited states.

Table 1 gives a summary of the present SAC-CI results for excitation energies, main configurations, oscillator strengths, and net charges in the excited states below 11 eV. All main configurations of the excited states except for 5^{1}T$_{2g}$ and 4^{1}T$_{1g}$ are single excitations from seven valence MOs having ligand nonbonding or metal–ligand bonding characters to the 3t$_{2g}$ LUMO with large amplitude at the 4d AOs of Mo. Both 5^{1}T$_{2g}$ and 4^{1}T$_{1g}$ states have 2t$_{1g} \rightarrow$ 9e$_g$ excitation characters. The 9e$_g$ MO also has large amplitude at the 4d AOs of Mo. Thus, these valence electronic transitions are roughly characterized as electron-transfer excitations from ligand to metal. In these excited states, the ionic character of the Mo–F bonds is much more relaxed than in the ground state. Actually, the calculated net charge on Mo is reduced from +1.26 to +0.85–+1.11.

In more details, the 2t$_{2g}$ and 7e$_g$ MOs have Mo–F π and σ character, respectively, although the other valence MOs are ligand nonbonding MOs. Therefore, the charge relaxations in the excited states of the 2t$_{2g} \rightarrow$ 3t$_{2g}$ and 7e$_g \rightarrow$ 3t$_{2g}$ excitations are smaller than those in the other states. Namely, the net charges on Mo in the former are from +1.00 to +1.11, and those in the latter from +0.85 to +0.95. However, because of their excitation nature from the bonding MOs, the geometry relaxations in the 2t$_{2g} \rightarrow$ 3t$_{2g}$ and 7e$_g \rightarrow$ 3t$_{2g}$ excited states are expected to be much greater than those in the other states.

In O_h symmetry, electronic transitions to the singlet T$_{1u}$ states are dipole-allowed. According to the SAC-CI results, we assign the three low-energy bands observed at 5.90, 6.54, and 7.12 eV to the lower three dipole-allowed ^{1}T$_{1u}$ states, respectively. Therewith, the energy discrepancies result in only −0.35, +0.08, and +0.12 eV, respectively. The calculated oscillator strengths of 0.0243, 0.0945, and 0.3549 agree with the measured intensities, respectively. These agreements might indicate that

TABLE 1: Summary for the Ground and Excited State of MoF$_6$

| | | SAC/SAC-CI | | | | experimental[a] | |
| | | | | net charge | | | |
state	main configuration	excitation energy (eV)	oscillator strength	Mo	F	excitation energy (eV)	intensity
X^{1}A$_{1g}$		0.000		+1.267	−0.205		
1^{1}A$_{2g}$	2t$_{1g}$ → 3t$_{2g}$	4.946	forbidden	+0.865	−0.144		
1^{1}T$_{2g}$	2t$_{1g}$ → 3t$_{2g}$	5.320	forbidden	+0.860	−0.143		
1^{1}T$_{1g}$	2t$_{1g}$ → 3t$_{2g}$	5.340	forbidden	+0.860	−0.143		
1^{1}T$_{2u}$	7t$_{1u}$ → 3t$_{2g}$	5.342	forbidden	+0.860	−0.143		
1^{1}T$_{1u}$	7t$_{1u}$ → 3t$_{2g}$	5.553	0.0243	+0.854	−0.142	5.90	weak
1^{1}A$_{1u}$	1t$_{2u}$ → 3t$_{2g}$	5.692	forbidden	+0.853	−0.142		
1^{1}E$_u$	1t$_{2u}$ → 3t$_{2g}$	5.693	forbidden	+0.852	−0.142		
2^{1}E$_u$	7t$_{1u}$ → 3t$_{2g}$	5.777	forbidden	+0.899	−0.150		
1^{1}A$_{2u}$	7t$_{1u}$ → 3t$_{2g}$	5.813	forbidden	+0.909	−0.152		
2^{1}T$_{2u}$	1t$_{2u}$ → 3t$_{2g}$	5.919	forbidden	+0.886	−0.148		
1^{1}E$_g$	2t$_{1g}$ → 3t$_{2g}$	6.016	forbidden	+0.893	−0.149		
2^{1}T$_{1u}$	1t$_{2u}$ → 3t$_{2g}$	6.624	0.0945	+0.894	−0.149	6.54	middle
2^{1}A$_{2u}$	6t$_{1u}$ → 3t$_{2g}$	6.672	forbidden	+0.912	−0.152		
3^{1}E$_u$	6t$_{1u}$ → 3t$_{2g}$	6.733	forbidden	+0.913	−0.152		
3^{1}T$_{2u}$	6t$_{1u}$ → 3t$_{2g}$	6.813	forbidden	+0.937	−0.156		
3^{1}T$_{1u}$	6t$_{1u}$ → 3t$_{2g}$	7.243	0.3549	+0.957	−0.160	7.12	strong
2^{1}T$_{2g}$	7a$_{1g}$ → 3t$_{2g}$	7.751	forbidden	+0.921	−0.153		
2^{1}E$_g$	2t$_{2g}$ → 3t$_{2g}$	8.908	forbidden	+1.066	−0.178	8.62	very weak
3^{1}T$_{2g}$	2t$_{2g}$ → 3t$_{2g}$	8.930	forbidden	+1.064	−0.177		
2^{1}T$_{1g}$	2t$_{2g}$ → 3t$_{2g}$	9.067	forbidden	+1.069	−0.178		
4^{1}T$_{2g}$	7e$_g$ → 3t$_{2g}$	9.491	forbidden	+1.021	−0.170	9.22	very weak
3^{1}T$_{1g}$	7e$_{1g}$ → 3t$_{2g}$	10.274	forbidden	+1.004	−0.167		
5^{1}T$_{2g}$	2t$_{1g}$ → 9e$_g$	10.428	forbidden	+0.940	−0.157		
2^{1}A$_{1g}$	2t$_{2g}$ → 3t$_{2g}$	10.749	forbidden	+1.117	−0.186		
4^{1}T$_{1g}$	2t$_{1g}$ → 9e$_g$	10.951	forbidden	+0.940	−0.157		

[a] Reference 6.

TABLE 2: Comparison between the Previous and Present Assignments

experiment[a]			Xα calculation[b]		SAC-CI calculation[c]		
ΔE (eV)	intensity	assign.	ΔE (eV)	assign.	ΔE (eV)	intensity	assign.
5.90	weak	2t$_{1g}$ → 3t$_{2g}$	5.87	2t$_{1g}$ → 3t$_{2g}$	5.55	0.0243	7t$_{1u}$ → 3t$_{2g}$
6.54	middle	7t$_{1u}$ → 3t$_{2g}$	6.60	7t$_{1u}$ → 3t$_{2g}$	6.61	0.0945	1t$_{2u}$ → 3t$_{2g}$
7.12	strong	1t$_{2u}$ → 3t$_{2g}$	7.32	6t$_{1u}$ → 3t$_{2g}$	7.26	0.3549	6t$_{1u}$ → 3t$_{2g}$
8.62	very weak	2t$_{2g}$ → 3t$_{2g}$	8.42	7a$_{1g}$ → 3t$_{2g}$	8.91	forbidden	2t$_{2g}$ → 3t$_{2g}$
9.22	very weak	4e$_g$ → 3t$_{2g}$	9.33	2t$_{2g}$ → 3t$_{2g}$	9.50	forbidden	4e$_g$ → 3t$_{2g}$

[a] Reference 6. [b] Reference 2. [c] Present study.

the geometry relaxations in these states are not so large owing to the excitations from the nonbonding MOs and do not lead to great red-shifts of the excitation energies.

Since there should be no ^{1}T$_{1u}$ states in the energy region from 7.7 to 10.9 eV, the next two bands experimentally observed at 8.62 and 9.22 eV with very weak intensities have to be assigned to the forbidden transitions. We have calculated the 2t$_{2g}$→ 3t$_{2g}$ and 7e$_g$ → 3t$_{2g}$ excitations in this energy region. Thus, we tentatively assign these two bands to the 2^{1}E$_g$ (2t$_{2g}$ → 3t$_{2g}$) and 4^{1}T$_{2g}$ (7e$_g$ → 3t$_{2g}$) states, respectively. Since these states are quadruple-allowed, they have the very weak intensities. Of course, Jahn−Teller effects and/or the vibronic coupling also contribute to the intensities of these states. There is only a small possibility that these electronic transitions at 8.62 and 9.22 eV bands might be assigned to Rydberg states, which appear at an energy of more than 11 eV in our calculations.

Finally, in Table 2, we compare the present assignment with those previously quoted.[2,6] The present assignment differs from them in several respects. In refs 2 and 6, the first weak-intensity peak was assigned to the dipole-forbidden 2t$_{1g}$ (HOMO) → 3t$_{2g}$ (LUMO) excitation. The present calculations yield the dipole-forbidden 2t$_{1g}$ → 3t$_{2g}$ (1^{1}A$_{2g}$, 1^{1}T$_{1g}$, and 1^{1}T$_{2g}$) excited states lower in energy than the first ^{1}T$_{1u}$ (allowed) excited state. However, if we follow this assignment for the first weak band (5.9 eV) to one of these dipole-forbidden states, it would result in the large discrepancies in both energy and intensity for the

successive electronic transitions. For example, the third ^{1}T$_{1u}$ state, which is calculated at 7.2 eV and with the largest oscillator strength, would have to be assigned to the very weak band at 8.62 eV. This is quite improbable and unreasonable. Thus, relying on our comprehensive theoretical data, we are naturally led to assign the three lower bands to the dipole-allowed transitions to the lower three ^{1}T$_{1u}$ states.

As to the two other very weak transitions at 8.62 and 9.22 eV, since we have calculated no allowed excited states from 7.2 up to 10.9 eV, we assign them to the forbidden excited states, in agreement with the previous studies but with different orbital origins. The X$_\alpha$ study assigned the band at 8.62 eV to the 7a$_{1g}$ → 3t$_{2g}$ state, of which the excitation energy was calculated to be 8.42 eV. However, for this ^{1}T$_{2g}$ state, the more accurate SAC-CI calculations yield the excitation energy of 7.75 eV, which is different by 0.9 eV.

B. Frozen Orbital Analysis of MoF$_6$: Excited-State Manifold. In the preceding section, we show that the accurate SAC-CI results for the singlet excited states of MoF$_6$ lead to the consistent and reasonable assignment of the experimental spectrum. There exist, however, many more states in the lower energy region and energetically close to the experimentally observed ones. These excited states cannot be neglected in understanding the photochemical behavior and excited-state dynamics, since internal conversions from the dipole-allowed to forbidden states occur easily. As shown in Table 1, most of

TABLE 3: Excitation Energy and Wave Function of the FZOA Method

category	state[a] gerade		ungerage		$^1\Delta E^{b,c,d}$			$^3\Delta E^{b,c,d}$			wave function Ψ^e
	*1	*2	*3	*4	A	B	C	A	B	C	
A	A_{1g}	A_{2g}	A_{1u}	A_{2u}	$\Delta\epsilon_{ia}$	$-J_{ia} + 2K_{ia}$	$2\{2(ai\lvert jb) - (ab\lvert ij)\}$	$\Delta\epsilon_{ia}$	$-J_{ia}$	$-2(ab\lvert ij)$	$1/\sqrt{3}(\Phi_i^a + \Phi_j^b + \Phi_k^c)$
E	E_g	E_g	E_u	E_u	$\Delta\epsilon_{ia}$	$-J_{ia} + 2K_{ia}$	$-\{2(ai\lvert jb) - (ab\lvert ij)\}$	$\Delta\epsilon_{ia}$	$-J_{ia}$	$(ab\lvert ij)$	$1/\sqrt{2}(\Phi_i^a - \Phi_j^b),$ $1/\sqrt{6}(\Phi_i^a + \Phi_j^b - 2\Phi_k^c)$
T_+	T_{2g}	T_{1g}	T_{2u}	T_{1u}	$\Delta\epsilon_{ia}$	$-J_{ib} + 2K_{ib}$	$-\{2(bi\lvert ja) - (ab\lvert ij)\}$	$\Delta\epsilon_{ia}$	$-J_{ib}$	$-(ab\lvert ij)$	$1/\sqrt{2}(\Phi_j^c + \Phi_k^b),$ $1/\sqrt{2}(\Phi_k^a + \Phi_i^c),$ $1/\sqrt{2}(\Phi_i^b + \Phi_j^a)$
T_-	T_{1g}	T_{2g}	T_{1u}	T_{2u}	$\Delta\epsilon_{ia}$	$-J_{ib} + 2K_{ib}$	$-\{2(bi\lvert ja) - (ab\lvert ij)\}$	$\Delta\epsilon_{ia}$	$-J_{ib}$	$(ab\lvert ij)$	$1/\sqrt{2}(\Phi_j^c - \Phi_k^b),$ $1/\sqrt{2}(\Phi_k^a - \Phi_i^c),$ $1/\sqrt{2}(\Phi_i^b - \Phi_j^a),$

^{a} *1. $t_{1g} \rightarrow t_{1g}$, $t_{2g} \rightarrow t_{2g}$, $t_{1u} \rightarrow t_{1u}$, $t_{2u} \rightarrow t_{2u}$ excitations; *2. $t_{1g} \rightarrow t_{2g}$, $t_{2g} \rightarrow t_{2g}$, $t_{1u} \rightarrow t_{2u}$, $t_{2u} \rightarrow t_{1u}$ excitations; *3. $t_{1g} \rightarrow t_{1u}$, $t_{2g}, \rightarrow t_{2u}$ $t_{1u} \rightarrow t_{1g}$, $t_{2u} \rightarrow t_{2g}$ excitations; *4. $t_{1g} \rightarrow t_{2u}$, $t_{2g} \rightarrow t_{1u}$, $t_{1u} \rightarrow t_{2g}$, $t_{2u} \rightarrow t_{1g}$ excitations. ^{b} $\Delta\epsilon_{ia}$ is the orbital energy difference between ith and ath MOs. ^{c} J and K are the Coulomb and exchange integrals, respectively. ^{d} $(kl\lvert mn)$ is a two-electron integral defined by $\int\int d\tau_1\, d\tau_2\, \phi_k^*(1)\, \phi_l(1)\, (1/r_{12})\phi_m^*(2)\, \phi_n(2)$. ^{e} Φ_l^d is a symmetry-adapted configuration state function of the excitation from ϕ_l to ϕ_d.
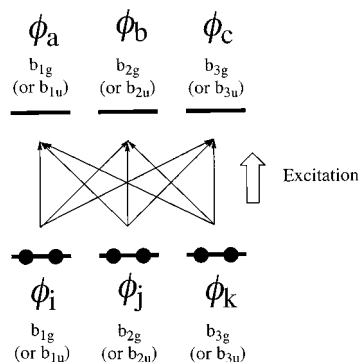
Figure 1. Illustration of the excitation from cubic to cubic degenerate MOs in O_h symmetry. The occupied ϕ_i, ϕ_j, and ϕ_k MOs are assigned to the b_{1g} (or b_{1u}), b_{2g} (or b_{2u}), and b_{3g} (or b_{3u}) species of D_{2h} subgroup symmetry, respectively. The unoccupied ϕ_a, ϕ_b, and ϕ_c MOs are also assigned to the three species of D_{2h} symmetry, respectively.

these states share the same main configuration between degenerate MOs. For example, 1^1A_{2g}, 1^1T_{1g}, 1^1T_{2g}, and 1^1E_g states all correspond to the $2t_{1g}$ (HOMO) $\rightarrow$ $3t_{2g}$ (LUMO) $(\pi \rightarrow \pi^*)$ excitation. Furthermore, we realize that only the highest state splits considerably from the other excited states within the same nature, except for the $7t_{1u} \rightarrow 3t_{2g}$ $(\sigma \rightarrow \pi^*)$ excitation. In particular, within the $2t_{2g} \rightarrow 3t_{2g}$ $(\pi \rightarrow \pi^*)$ excitation, the highest state 2^1A_{1g} is about 1.7 eV higher in energy than the second highest state 3^1T_{2g}.

In this section, we try to understand the origin of the energy orderings and splittings of the excited states within the same excitation nature. We have recently proposed a simple theoretical scheme, the FZOA method, to solve this problem.[15]

First, we briefly explain the splitting scheme in the FZOA method. In O_h symmetry, excitations from cubic to cubic degenerate MOs lead to four distinct excited states. Table 3 summarizes wave functions and energies for all kinds of states which arise from excitations between cubic degenerate MOs. The four distinct states are categorized into one nondegenerate A state, one quadratic E state, and two cubic T_+ and T_- states, respectively. Here, we define (ϕ_i, ϕ_j, ϕ_k) and (ϕ_a, ϕ_b, ϕ_c) as occupied and unoccupied MOs, respectively, as shown in Figure 1.

In the FZOA method, we write the singlet- and triplet-excitation energies in the following partitioned form

$$\Delta E = A + B + C \qquad (1)$$

where A is the orbital energy difference, B the $-J + 2K$ $(-J$ for triplet states) term, and C a four-index repulsion integral
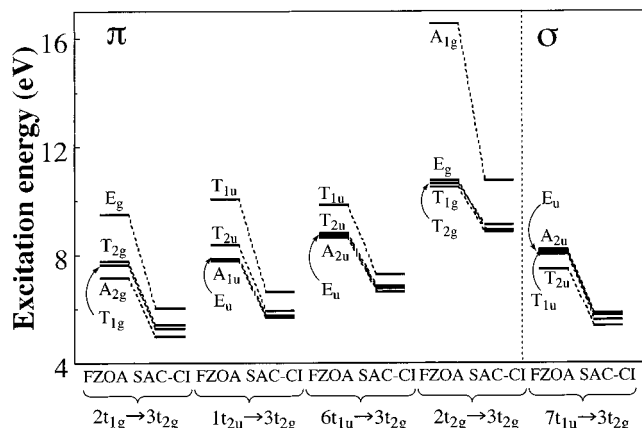
Figure 2. Comparison of the excitation energies of the MoF$_6$ calculated by the FZOA and SAC-CI methods.

term. Explicit formulas for the A, B, and C terms are shown in Table 3. Note that the C term is the most specific to the excitation between the degenerate MOs. The A term, of course, does not bring any energy splitting for the four states determining only the absolute value of the excitation energy. The B term brings about the energy splitting between (A, E) and (T_+, T_-) pairs. The C term eventually yields the energy splittings within the individual pairs (A, E) and (T_+, T_-).

Figure 2 shows the energy levels for the $2t_{1g} \rightarrow 3t_{2g}$, $1t_{2u} \rightarrow 3t_{2g}$, $6t_{1u} \rightarrow 3t_{2g}$, $2t_{2g} \rightarrow 3t_{2g}$, and $7t_{1u} \rightarrow 3t_{2g}$ excitations calculated by the FZOA and the SAC-CI methods. The $6t_{1u} \rightarrow 3t_{2g}$ and $7t_{1u} \rightarrow 3t_{2g}$ excitations, which have already been discussed in ref 15, are shown again in order to compare them with the other excitations. The $2t_{1g}$, $1t_{2u}$, $6t_{1u}$, and $2t_{2g}$ MOs have π character, whereas the $7t_{1u}$ MO has σ character.

Since the FZOA method actually corresponds to SE-CI calculations within the minimum configuration space [3 × 3], it cannot give quantitatively accurate results. However, we notice from Figure 2 that the orderings of the four states calculated by the FZOA method consistently agree with those by the SAC-CI method, except for the $2t_{2g} \rightarrow 3t_{2g}$ excitation. Even for the $2t_{2g} \rightarrow 3t_{2g}$ excitation, the intrapair orderings (i.e., between ^1E_g and $^1A_{1g}$, and between $^1T_{1g}$ and $^1T_{2g}$ states) are the same as those of the SAC-CI results. For gerade states, the energy splittings between E and A states are larger than those between T_+ and T_- states. On the other hand, the energy splittings between ^1E_u and $^1A_{1u}$ (or $^1A_{2u}$) are smaller than those between $^1T_{1u}$ and $^1T_{2u}$ states. These qualitative relationships for the energy orderings seem to hold in the FZOA results as well as in the SAC-CI calculations. Thus, the energy orderings

TABLE 4: Summary of the Values of MO Integrals for MoF$_6$ in Table 3

| Main Configuration	State	A Term (eV) ε_i	ε_a	Total	B Term (eV) J_{ia} / J_{ib}	K_{ia} / K_{ib}	Total	C Term (eV) (ailjb)/(bilja)	(ablij)	Total	Transition dipole $\langle\Phi_{ia}|r|0\rangle$ / $\langle\Phi_{ib}|r|0\rangle$	Total
π character												
$2t_{1g}\rightarrow 3t_{2g}$	$^1A_{2g}$	-18.3457	-3.1640	15.1817	8.3992	0.9544	-6.4904	-0.4086	-0.0477	-1.5390	0.0	0.0
	^1E_g				7.5708	0.0353	-7.5002	-0.0347		0.7695		0.0
	$^1T_{1g}$									-0.0217		0.0
	$^1T_{2g}$									0.0217		0.0
$1t_{2u}\rightarrow 3t_{2g}$	$^1A_{1u}$	-19.0187	-3.1640	15.8547	8.1969	0.0656	-8.0657	-0.0328	-0.0518	-0.0276	0.0	0.0
	^1E_u				7.6875	0.5170	-6.6535	-0.4482		0.0138		0.0
	$^1T_{1u}$									0.8446	1.0702	1.5135
	$^1T_{2u}$									-0.8446		0.0
$6t_{1u}\rightarrow 3t_{2g}$	$^1A_{2u}$	-19.8194	-3.1640	16.6554	8.0803	0.0517	-7.9769	0.0298	0.0816	-0.0440	0.0	0.0
	^1E_u				8.1323	0.3891	-7.3541	0.3101		0.0220		0.0
	$^1T_{1u}$									0.5386	0.7587	1.0729
	$^1T_{2u}$									-0.5386		0.0
$2t_{2g}\rightarrow 3t_{2g}$	$^1A_{1g}$	-22.1600	-3.1640	18.9960	9.4605	1.5579	-6.3447	1.0373	0.1421	3.8650	0.0	0.0
	^1E_g				8.6031	0.1218	-8.3595	0.1210		-1.9325		0.0
	$^1T_{1g}$									-0.0999		0.0
	$^1T_{2g}$									0.0999		0.0
σ character												
$7t_{1u}\rightarrow 3t_{2g}$	$^1A_{2u}$	-18.7537	-3.1640	15.5897	7.5155	0.0260	-7.4635	0.0151	0.0046	0.0514	0.0	0.0
	^1E_u				8.3439	0.2327	-7.8785	0.1464		-0.0257		0.0
	$^1T_{1u}$									0.2882	0.6408	0.9061
	$^1T_{2u}$									-0.2882		0.0
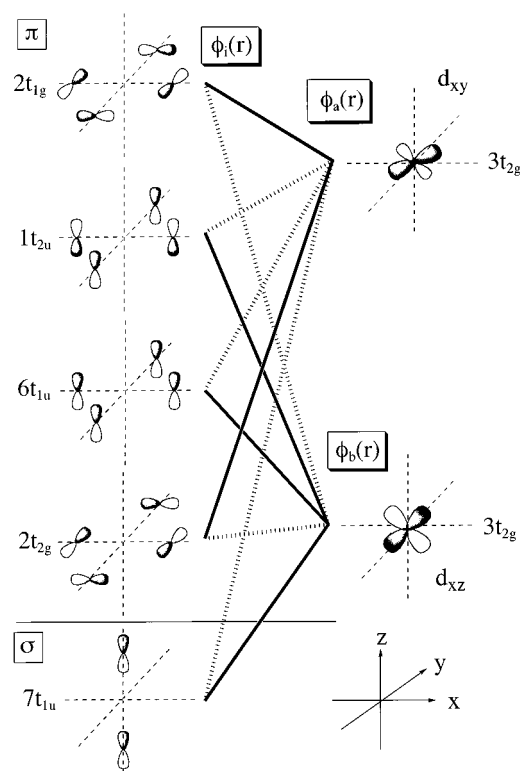
Figure 3. Combination of the orbitals of MoF$_6$ for the transition density. The solid and dotted lines are large and small overlaps between them, respectively.

and splittings calculated by the FZOA method are kept in the accurate SAC-CI calculations.

This in turn allows us to use the much simpler FZOA method to try to understand the complicated excited states of MoF$_6$. Table 4 lists the numerical data for the orbital energies and two-electron integrals appearing in Table 3. The absolute values of Coulomb integrals are larger than those of the exchange and four-index two-electron integrals. For excitations from the σ-character 7t$_{1u}$ MO, the energy difference between J_{ia} and J_{ib} is dominant to the ordering caused by the B term. The origin of this large energy difference between J_{ia} and J_{ib} in this case has been discussed in ref 15 by using electron density. On the other hand, in the cases of π-character MOs, the B term is determined by the exchange integrals. One finds that the exchange integrals, K_{ia} and K_{ib}, differ from each other by 1 order of magnitude in every cases. The integrals $(ai|jb)$ and $(bi|ja)$, which are more important than $(ab|ij)$ integrals for the energy splittings by the C term, also differ from each other by 1 order of magnitude. Furthermore, the energy orderings of these integrals are the same. Namely, when $K_{ia} < K_{ib}$, one finds $(ai|jb) > (bi|ja)$. Now, these integrals involve the transition density $\phi_a{}^*(r)\ \phi_i(r)$ or $\phi_b{}^*(r)\ \phi_i(r)$. The transition densities $\phi_j{}^*(r)\ \phi_b(r)$ and $\phi_j{}^*(r)\ \phi_a(r)$ involved in $(ai|jb)$ and $(bi|ja)$ have, except for the rotation of the coordinate axis, the same distributions as $\phi_a{}^*(r)\ \phi_i(r)$ and $\phi_b{}^*(r)\ \phi_i(r)$, respectively. Therefore, how the energy orderings of these integrals come about should be understood by analyzing these transition densities, which correspond to the spatial distributions of the overlaps between the two relevant MOs such as $\phi_a(r)$ and ϕ_i-(r).

Figure 3 schematically shows the respective combinations, $\phi_a{}^*(r)\ \phi_i(r)$ and $\phi_b{}^*(r)\ \phi_i(r)$, in the cases of (2t$_{1g}$, 1t$_{2u}$, 6t$_{1u}$, 2t$_{2g}$, and 7t$_{1u}$) → 3t$_{2g}$ excitations. We now discuss the case of the 2t$_{1g}$ MOs as an example. The $\phi_i(r)$ MO of b$_{1g}$ symmetry (in D_{2h} subset) has a maximum amplitude on the xy-plane (see
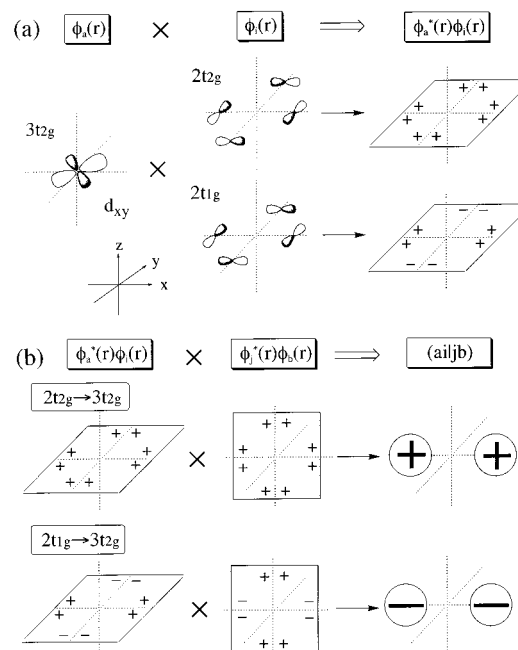
Figure 4. Illustration of the calculation of two-electron integrals $(ai|jb)$ for the 2t$_{2g}$ → 3t$_{2g}$ and 2t$_{1g}$ → 3t$_{2g}$ excitations. Plus and minus signs of the transition densities are determined by the phases of the two MOs (a) and those of the integrals by the phases of the two transition densities (b).

Figure 3). On the other hand, $\phi_a(r)$ and $\phi_b(r)$ MOs of b$_{1u}$ and b$_{2u}$ symmetries (D_{2h}) have maximum amplitudes on the xy- and xz-planes, respectively. Therefore, the pair of $\phi_i(r)$ and $\phi_a(r)$ has a larger overlap than that of $\phi_i(r)$ and $\phi_b(r)$. In Figure 3, we show the overlap difference between the two MOs by using solid (large) and broken (small) lines, respectively. It turns out that the combinations $\phi_a{}^*(r)\ \phi_i(r)$ and $\phi_b{}^*(r)\ \phi_i(r)$ have the larger overlaps for the gerade−gerade and ungerade−gerade pairs, respectively. This causes the large energy difference between $(ai|jb)$ and $(bi|ja)$ integrals and further, in turn, the large difference of the energy splittings between E and A and between T$_+$ and T$_-$. Since this fact is also at the origin of the large difference between K_{ia} and K_{ib}, we formulate the following general rule for the cases of π-character MOs:

"States which split greater lie at higher energy than those whose splittings are smaller."

Moreover, since transition densities determine the oscillator strengths, it turns out that the energetically highest excited state within the same excitation nature is dipole-allowed. Table 4 also lists the numerical data for the transition dipole moments of the configuration-state-function basis. $\langle\Phi_i{}^a|r|0\rangle$ and $\langle\Phi_i{}^b|r|0\rangle$ of the 2t$_{1g}$ → 3t$_{2g}$ and 2t$_{2g}$ → 3t$_{2g}$ excitations always vanish to zero. In the remaining excitations, 7t$_{1u}$ → 3t$_{2g}$, 1t$_{2u}$ → 3t$_{2g}$, and 6t$_{1u}$ → 3t$_{2g}$, $\langle\Phi_i{}^b|r|0\rangle$ is nonzero. However, the transition dipole moments of ^{1}T$_{2u}$ states result in zero because of the exact cancellation between $\langle\Phi_j{}^a|r|0\rangle$ and $\langle\Phi_i{}^b|r|0\rangle$.

While Coulomb and exchange integrals are always positive, $(ai|jb)$ and $(bi|ja)$ four-index integrals are not. For example, values of $(ai|jb)$ for the 2t$_{1g}$ → 3t$_{2g}$ and 2t$_{2g}$ → 3t$_{2g}$ excitations turn out to be −0.40 and 1.03, respectively. This difference brings about the different ordering between A and E states; namely, ^{1}E$_g$ > ^{1}A$_{2g}$ for 2t$_{1g}$ → 3t$_{2g}$ and ^{1}A$_{1g}$ > ^{1}E$_g$ for 2t$_{2g}$ → 3t$_{2g}$. It is easy to explain how the sign of the two-electron integrals comes about, when we consider the phases of the relevant transition densities.

Figure 4 shows a schematic illustration for the evaluation of $(ai|jb)$ integrals. In the upper part (a), the combination of ϕ_a-

Electronic Structures of MoF$_6$ and MoOF$_4$

J. Phys. Chem. A, Vol. 102, No. 11, 1998 **2039**
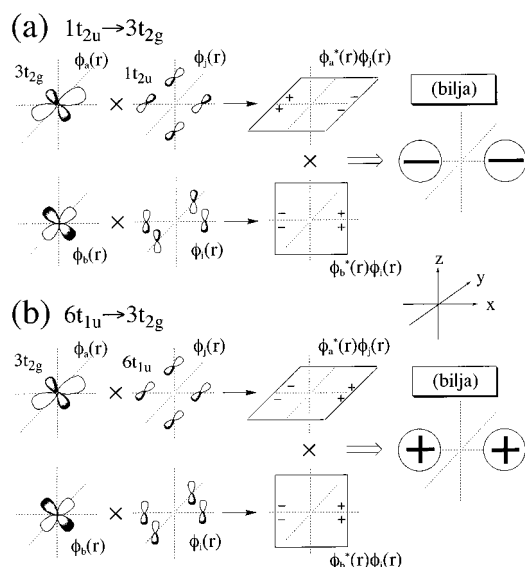
Figure 5. Illustration of the calculation of two-electron integrals ($bi|ja$) for the (a) $1t_{2u} \rightarrow 3t_{2g}$ and (b) $6t_{1u} \rightarrow 3t_{2g}$ excitations. Plus and minus signs of the transition densities are determined by the phases of the two MOs and those of the integrals by the phases of the two transition densities.

(r) and $\phi_i(r)$ giving the transition density $\phi_a^*(r)\phi_i(r)$ is depicted. In the lower part (b), the combination of $\phi_a^*(r)\phi_i(r)$ and $\phi_j^*(r)\phi_b(r)$ leading to $(ai|jb)$ integrals is sketched. Now, since the integration involves a short-range operator r_{12}^{-1}, the sign of the $(ai|jb)$ is determined by the closest pair of the maximum amplitudes of the two transition densities. In the case of the $2t_{1g} \rightarrow 3t_{2g}$ excitation, the closest pairs are those near the x-axis. There, the signs of the maximum amplitudes of $\phi_a^*(r)\phi_i(r)$ and $\phi_j^*(r)\phi_b(r)$ are opposite to each other. Therefore, the integral obtains a negative value. On the other hand, since the maximum amplitudes of $\phi_a^*(r)\phi_i(r)$ and $\phi_j^*(r)\phi_b(r)$ for the $2t_{2g} \rightarrow 3t_{2g}$ excitation are positive, the integral obtains a positive value. Moreover, since there is no cancellation owing to the opposite signs, the absolute value of $(ai|jb)$ becomes greater for the $2t_{1g} \rightarrow 3t_{2g}$ excitation than those for the other cases. This is a reason for the largest energy splitting between the 2^1A_{1g} and 2^1E_g states.

The values of the $(bi|ja)$ integral for the $1t_{2u} \rightarrow 3t_{2g}$ and $6t_{1u} \rightarrow 3t_{2g}$ excitations are -0.45 and 0.31 eV, respectively. These different values and signs of the relevant integrals are also explained in Figure 5, which shows the schematic illustration for qualitatively evaluating the $(bi|ja)$ integrals. Therein, the upper (a) and lower (b) parts refer to the $(bi|ja)$ integrals for $1t_{2u} \rightarrow 3t_{2g}$ and $6t_{1u} \rightarrow 3t_{2g}$ excitations, respectively. The transition densities, $\phi_a^*(r)\phi_i(r)$ and $\phi_j^*(r)\phi_b(r)$, shown in Figure 5 have large amplitudes along the x-axis, but there they show both positive and negative signs. For the $1t_{2u} \rightarrow 3t_{2g}$ excitation, they have opposite signs, and the integral results negative. On the other hand, since they have same signs for the $6t_{1u} \rightarrow 3t_{2g}$ excitation, the integral results positive.

The T_+ and T_- states of the $1t_{2u} \rightarrow 3t_{2g}$ and $6t_{1u} \rightarrow 3t_{2g}$ excitations appear reversibly as the effect of the C term, as shown in Table 3. However, on account of the opposite signs of the $(bi|ja)$ integrals, the energy orderings of the T_{1u} and T_{2u} states for both excitations become the same; namely, $T_{1u} > T_{2u}$.

Finally, using the FZOA method, we are able to predict the energy orderings and splittings of the *triplet* states, which are not calculated by the SAC-CI method in the present study. In Table 5, the singlet- and triplet-excitation energies of MoF$_6$ estimated by the FZOA method are reported for comparison. As shown for the singlet states in Figure 2, the FZOA results

of the excited-state energies do not achieve quantitative accuracy. However, as far as the state orderings are of concern, they seem to reproduce the outcome of more accurate CI calculations. It is perhaps worthy to note, in Table 5, that all triplet-excitation energies appear systematically lower than those corresponding to the singlet states. This is, of course, because of the lack of the exchange-integral terms for the triplet-excitation energies in the FZOA expression. An aspect of the FZOA method closely parallels the well-known Hund's rule,[25] the atomic *Aufbau* principle. However, the FZOA method further yields that the relative orderings of the triplet states having the excitation nature are different from those of the singlet states and the energy splittings appear smaller. This is because the triplet-excitation energies in the FZOA method do not include exchange integrals, K_{ia} and K_{ib}, and four-index ones, $(ai|jb)$ and $(bi|ja)$.

The analysis of the excited states of MoF$_6$ performed in this section, which uses only the symmetries and characters of the relevant MOs, has led to a *microscopic* understanding and rationalization of the state orderings and energy splittings obtained in much more complicated CI results. The qualitative relationships found here should be suitable for any systems in O_h symmetry. Moreover, we may state the following general rule for any molecules in any symmetries:

"For the singlet-excited states related with π-character MOs, the dipole-allowed state is located at the highest level and is greatly split from the other states with the same nature."

C. SAC-CI Calculations of MoOF$_4$: Ground and Excited States. Table 6 shows orbital energies and characters of MoOF$_4$. Therein, only valence occupied and lower unoccupied MOs are reported. All valence occupied MOs have large amplitudes at the ligand AOs. 10e and 15a$_1$ MOs have, in particular, larger amplitudes at the 2p AOs of O, whereas other occupied MOs have larger coefficients at the 2p AOs of F atoms. On the other hand, unoccupied 3b$_2$, 11e, 20a$_1$, and 8b$_1$ MOs are mainly composed of the 4d AOs of Mo with the Mo−ligand antibonding nature.

Table 6 also compares with the symmetries of valence occupied and two virtual MOs of MoF$_6$. Since MoOF$_4$ (C_{4v}) is a lower symmetry than MoF$_6$ (O_h), highly degenerate MOs in the latter split in the former. e$_g$, t$_{2g}$, t$_{1u}$, t$_{2u}$, a$_{1g}$, and t$_{1g}$ symmetry elements correspond to those of the C_{4v} as follows:

$$e_g = b_1 + a_1, \quad t_{2g} = b_2 + e, \quad t_{1u} = a_1 + e$$

$$t_{2u} = b_1 + e, \quad a_{1g} = a_1, \quad t_{1g} = a_2 + e$$

MoF$_6$ has three more valence occupied MOs than MoOF$_4$. From the orbital characters, there are only a few cases in which we can correspond the MOs of MoF$_6$ to those of MoOF$_4$. The gerade MOs are quite direct as shown in Table 6. On the other hand, it is difficult to make direct correspondence to 8e and 9e MOs because of the orbital mixing, although 6t$_{1u}$, 1t$_{2u}$, and 7t$_{1u}$ MOs of MoF$_6$ are related to 8e, 5b$_1$, 9e, and 14a$_1$ MOs of MoOF$_4$.

Similar to MoF$_6$, the formal charge of +6 attributable to Mo in MoOF$_4$ is greatly reduced by the chemical bonding and the electron correlation giving covalent characters to Mo−F and Mo−O bonds. However, the formal charge on Mo is reduced in MoOF$_4$ to a minor extent. The net charge on Mo is calculated to be +2.55 at the SCF level, which, by inclusion of the electron correlation by the SAC method, is further decreased to +2.33. This charge is about twice as large as that of MoF$_6$ (+1.27), which clearly indicates that MoOF$_4$ is more ionic than MoF$_6$.

TABLE 5: Comparison between the Singlet and Triplet Excitation Energies Calculated by the FZOA Method

	singlet		triplet	
main configuration	state	excitation energy (eV)	state	excitation energy (eV)
π character				
$2t_{1g} \rightarrow 3t_{2g}$	$^1A_{2g}$	7.1523 (0.0000)	^3E_g	6.7348 (0.0000)
	$^1T_{1g}$	7.6600 (0.4121)	$^3A_{2g}$	6.8779 (0.1431)
	$^1T_{2g}$	7.7030 (0.6463)	$^3T_{2g}$	7.5632 (0.8284)
	^1E_g	9.4608 (2.3085)	$^3T_{1g}$	7.6586 (0.9238)
$1t_{2u} \rightarrow 3t_{2g}$	$^1A_{1u}$	7.7614 (0.0000)	^3E_u	7.6060 (0.0000)
	^1E_u	7.8028 (0.0414)	$^3A_{1u}$	7.7614 (0.1554)
	$^1T_{2u}$	8.3566 (0.4916)	$^3T_{2u}$	8.1154 (0.5094)
	$^1T_{1u}$	10.0458 (2.3880)	$^3T_{1u}$	8.2190 (0.6130)
$6t_{1u} \rightarrow 3t_{2g}$	$^1A_{2u}$	8.6345 (0.0000)	$^3A_{2u}$	8.4119 (0.0000)
	^1E_u	8.7005 (0.0660)	$^3T_{1u}$	8.4415 (0.0296)
	$^1T_{2u}$	8.7627 (0.1282)	$^3T_{2u}$	8.6047 (0.1928)
	$^1T_{1u}$	9.8399 (1.2054)	^3E_u	8.6567 (0.2448)
$2t_{2g} \rightarrow 3t_{2g}$	$^1T_{1g}$	10.5366 (0.0000)	$^3A_{1g}$	9.2513 (0.0000)
	^1E_g	10.7188 (0.1822)	^3E_g	9.6776 (0.4263)
	$^1T_{2g}$	10.7364 (0.1998)	$^3T_{1g}$	10.2508 (0.9995)
	$^1A_{1g}$	16.5163 (5.9797)	$^3T_{2g}$	10.5350 (1.2837)
σ character				
$7t_{1u} \rightarrow 3t_{2g}$	$^1T_{2u}$	7.4230 (0.0000)	$^3T_{1u}$	7.2412 (0.0000)
	$^1T_{1u}$	7.9994 (0.5764)	$^3T_{2u}$	7.2504 (0.0092)
	^1E_u	8.1005 (0.6775)	$^3A_{2u}$	8.0650 (0.8238)
	$^1A_{2u}$	8.1776 (0.7546)	^3E_u	8.0788 (0.8376)

[a] Energy differences from the lowest excited states with the same main configurations are shown in parentheses.

TABLE 6: Orbital Energies and Characters of the HF Wave Function for MoOF$_4$ and Correspondence to MoF$_6$

	MoOF$_4$		
MoF$_6$	symmetry	character[a]	orbital energy (eV)
		Occupied Orbitals	
$7e_g$	$4b_1$	F (2p) + Mo (4d); σ	-21.8097
	$13a_1$	O (2p) + Mo (4d), F (2p) + Mo (4d); σ	-21.1924
$2t_{2g}$	$2b_2$	F (2p) (+ Mo (4d)); π	-20.9615
	$7e$	F (2p) + Mo (4d), O (2p) + Mo (4d); π	-20.6806
$7a_{1g}$	$14a_1$	F (2p) + Mo (5s); π	-19.2725
$6t_{1u}$	$8e$	F (2p); σ, π	-18.7569
$1t_{2u}$	$5b_1$	F (2p); π	-18.2747
$7t_{1u}$	$9e$	F (2p); σ, π	-18.1666
	$15a_1$	O (2p) + Mo (5s); σ	-17.8673
$2t_{1g}$	$1a_2$	F (2p); π	-17.5683
	$10e$	O (2p) (+ Mo (5p)), F (2p) (+ Mo (5p)); π	-16.6165
		Unoccupied Orbitals	
$3t_{2g}$	$3b_2$	Mo (4d) ($-$F (2p)); π	-2.0920
	$11e$	Mo (4d) $-$ O (2p); π	-0.9453
$9e_g$	$20a_1$	Mo (4d) ($-$ O (2p)), Mo (4d) ($-$ F (2p)); σ	0.8824
	$8b_1$	Mo (4d) ($-$ F (2p)); σ	2.2101

[a] + and $-$ denote bonding and antibonding combinations, respectively.

This is mainly due to different 5s populations of Mo in the two cases (1.58 and 0.41 for MoF$_6$ and MoOF$_4$, respectively).

Table 7 presents a summary of the SAC-CI results for excitation energies (up to 11 eV), main configurations, oscillator strengths, and net charges. Reported are also the available experimental data of Levason et al.[8] All main configurations of the excited states lower than 10.8 eV are single excitations to $3b_2$, $11e$, $20a_1$, and $8b_1$ virtual MOs, whose amplitudes are comparatively larger at the 4d AOs of Mo. These electronic transitions are thus all characterized as electron-transfer excitations from ligand to metal. Since MoOF$_4$ has C_{4v} symmetry, transitions to ^{1}E and ^{1}A$_1$ states are dipole-allowed. According to the SAC-CI results, we assign the electronic transitions observed at 4.86 and 5.48 eV to the 1^1E and 2^1E states, respectively. The errors with respect to the experiment are reasonably small (within 0.3 eV). With respect to the ground state, these excitations bring large changes of the charges on

oxygen and on fluorine, respectively. Therefore, they may be described as electron-transfer of O $\rightarrow$ Mo and F $\rightarrow$ Mo, respectively. This assignment parallels that in ref 8, although there the energy of the first excited state (O $\rightarrow$ Mo) has been underestimated by about 1 eV. The calculated intensities for the excited states of MoOF$_4$ also agree with the experiment. Thus, the present assignment is more reasonable and reliable. Although no experimental data are available, we further predict three strong bands around 6.4, 7.4, and 8.3 eV due to the 3^1E, 2^1A$_1$, and 7^1E states, respectively.

D. Frozen Orbital Analysis of MoOF$_4$: Excited-State Manifold. In section III.B, we discuss the orderings and splittings of the excited states of MoF$_6$, which are related to the excitations between cubic degenerate MOs, by using the FZOA method. Since MoOF$_4$ has C_{4v} symmetry, which is lower than O_h of MoF$_6$, the cubic degenerate MOs in O_h split to one nondegenerate and one quadratic degenerate MOs in C_{4v}. For

TABLE 7: Summary for the Ground and Singlet Excited States of MoOF$_4$

| state	main configuration	excitation energy (eV)	oscillator strength	net charge Mo	net charge O	net charge F	experimental[a] excitation energy (eV)	experimental[a] oscillator strength
XA$_1$				+2.33	−0.63	−0.43		
1E	10e → 3b$_2$	4.659	0.0056	+1.97	−0.32	−0.41	4.86	middle
1B$_1$	1a$_2$ → 3b$_2$	5.410	forbidden	+1.92	−0.68	−0.31		
1B$_2$	15a$_1$ → 3b$_2$	5.617	forbidden	+1.99	−0.36	−0.41		
2E	9e → 3b$_2$	5.754	0.0378	+1.88	−0.73	−0.29	5.48	strong
1A$_2$	5b$_1$ → 3b$_2$	5.778	forbidden	+1.90	−0.70	−0.30		
2A$_2$	10e → 11e	5.959	forbidden	+2.10	−0.46	−0.41		
2B$_2$	10e → 11e	6.109	forbidden	+2.12	−0.44	−0.42		
2B$_1$	10e → 11e	6.215	forbidden	+2.11	−0.50	−0.40		
3E	8e → 3b$_2$	6.398	0.0766	+1.92	−0.70	−0.30		
3B$_2$	14a$_1$ → 3b$_2$	6.851	forbidden	+1.94	−0.67	−0.32		
4E	15a$_1$ → 11e	6.892	0.0002	+2.15	−0.46	−0.42		
5E	1a$_2$ → 11e	7.225	0.0005	+1.95	−0.85	−0.28		
2A$_1$	10e → 11e	7.339	0.1266	+2.07	−0.58	−0.37		
3B$_1$	9e → 11e	7.606	forbidden	+1.92	−0.84	−0.27		
3A$_1$	9e → 11e	7.660	0.0059	+1.93	−0.83	−0.27		
3A$_2$	9e → 11e	7.669	forbidden	+1.95	−0.84	−0.28		
4B$_2$	9e → 11e	7.681	forbidden	+1.96	−0.84	−0.28		
6E	5b$_1$ → 11e	8.031	0.0458	+2.01	−0.73	−0.32		
7E	7e → 3b$_2$	8.264	0.0722	+2.03	−0.70	−0.33		
8E	10e → 20a$_1$	8.404	0.0113	+2.05	−0.52	−0.38		
4A$_1$	8e → 11e	8.430	0.0063	+2.02	−0.76	−0.31		
5B$_2$	8e → 11e	8.455	forbidden	+1.96	−0.79	−0.29		
4B$_1$	8e → 11e	8.477	forbidden	+1.96	−0.83	−0.28		
4A$_2$	8e → 11e	8.501	forbidden	+1.95	−0.83	−0.28		
6B$_2$	13a$_1$ → 3b$_2$	8.646	forbidden	+2.01	−0.62	−0.35		
5A$_1$	2b$_2$ → 3b$_2$	8.891	0.0239	+2.02	−0.74	−0.32		
5A$_2$	4b$_1$ → 3b$_2$	8.936	forbidden	+2.01	−0.72	−0.32		
9E	14a$_1$ → 11e	9.053	0.0619	+2.00	−0.82	−0.30		
10E	10e → 8b$_1$	9.368	0.0017	+2.02	−0.35	−0.42		
6A$_2$	1a$_2$ → 20a$_1$	9.633	forbidden	+1.76	−0.87	−0.22		
7B$_2$	1a$_2$ → 8b$_1$	9.729	forbidden	+1.93	−0.71	−0.30		
5B$_1$	7e → 11e	9.993	forbidden	+2.10	−0.75	−0.34		
11E	9e → 20a$_1$	10.020	0.0001	+1.90	−0.83	−0.27		
6A$_2$	7e → 11e	10.195	forbidden	+2.11	−0.79	−0.33		
6A$_1$	5b$_1$ → 8b$_1$	10.237	0.0194	+1.98	−0.71	−0.32		
12E	13a$_1$ → 11e	10.288	0.0006	+2.02	−0.78	−0.31		
6B$_1$	5b$_1$ → 20a$_1$	10.316	forbidden	+1.77	−0.78	−0.25		
8B$_2$	7e → 11e	10.368	forbidden	+2.13	−0.77	−0.34		
13E	2b$_2$ → 11e	10.477	0.0172	+2.03	−0.80	−0.31		
7B$_1$	15a$_1$ → 8b$_1$	10.525	forbidden	+2.07	−0.51	−0.39		
7A$_1$	7e → 11e	10.576	0.2338	+1.98	−0.71	−0.32		
14E	2b$_2$ → 11e	10.835	0.0747	+1.98	−0.77	−0.30		

[a] Reference 8.

example, the 3t$_{2g}$ and 2t$_{1g}$ MOs of MoF$_6$ correspond to the (11e, 3b$_2$) and (10e, 1a$_2$) MOs of MoOF$_4$, respectively, as shown in Figure 6. Therefore, the excited states, A$_{2g}$, E$_g$, T$_{1g}$, and T$_{2g}$, derived from the 2t$_{1g}$ → 3t$_{2g}$ excitations also split in MoOF$_4$; namely, the 10e → 3b$_2$, 1a$_2$ → 3b$_2$, 10e → 11e, and 1a$_2$ → 11e excitations derive the E, B$_1$ (A$_1$, B$_1$, A$_2$, B$_2$), and E states, respectively. The excited states corresponding between O$_h$ and C$_{4v}$ symmetries in Figure 6 are connected with the broken lines.

It is seen therein that two ^{1}E states of MoOF$_4$ are derived from ^{1}T$_{1g}$ and ^{1}T$_{2g}$ states. There exists, in general, no one-to-one correspondence between the O$_h$ and C$_{4v}$ excited states because of partial or complete symmetry mixing. For example, although ^{1}A$_1$, ^{1}B$_2$, and ^{1}A$_2$ states derive from ^{1}E$_g$, ^{1}T$_{1g}$, and ^{1}T$_{2g}$ symmetries, respectively, ^{1}B$_1$ and ^{1}E states have 2-fold origins. Indeed, the ^{1}B$_1$ states are connected to both ^{1}E$_g$ and ^{1}A$_{2g}$ symmetries, as well as the ^{1}E states to both ^{1}T$_{1g}$ and ^{1}T$_{2g}$ symmetries. The energy splittings of the 10e → 3b$_2$, 1a$_2$ → 3b$_2$, 10e → 11e, and 1a$_2$ → 11e excitations arise mainly due to the orbital energy differences. For example, the energy gap of the two ^{1}E states is approximately given by orbital energy differences. However, the energy orderings and splittings of the four states, ^{1}A$_1$, ^{1}B$_1$, ^{1}A$_2$, and ^{1}B$_2$, for the 10e → 11e

excitation, cannot be explained by the orbital energy differences. Then, we apply the FZOA method to the e → e excitations.

Let us define (ϕ_i, ϕ_j) and (ϕ_a, ϕ_b) as quadratic degenerate (e symmetry) occupied and unoccupied MOs, respectively. The excitation energies for the e → e transitions are also composed of the three energy terms defined in eq 1 in section III.B. The B term gives rise to the energy splitting between (A$_1$, B$_1$) and (A$_2$, B$_2$) pairs. The C term instead brings about the energy splitting between A$_1$ and B$_1$ states as well as that between A$_2$ and B$_2$ states.

Figure 7 shows the energy levels for the (10e, 7e, 9e, and 8e) → 11e excitations calculated by the FZOA and the SAC-CI methods. As noticed for MoF$_6$, the energy ordering of the four states for the 10e → 11e excitation calculated by the FZOA method results in the same as that obtained by SAC-CI calculation. For the 7e → 11e excitation, the intrapair orderings of (^{1}A$_1$, ^{1}B$_1$) and (^{1}A$_2$, ^{1}B$_2$), which are brought about by the C term, are the same as the SAC-CI results. Although quite different orderings appear for the 9e → 11e and 8e → 11e excitations, the energy splittings are very small compared with those of the 10e → 11e and 7e → 11e states. The largest energy

2042 *J. Phys. Chem. A, Vol. 102, No. 11, 1998*

Nakai et al.
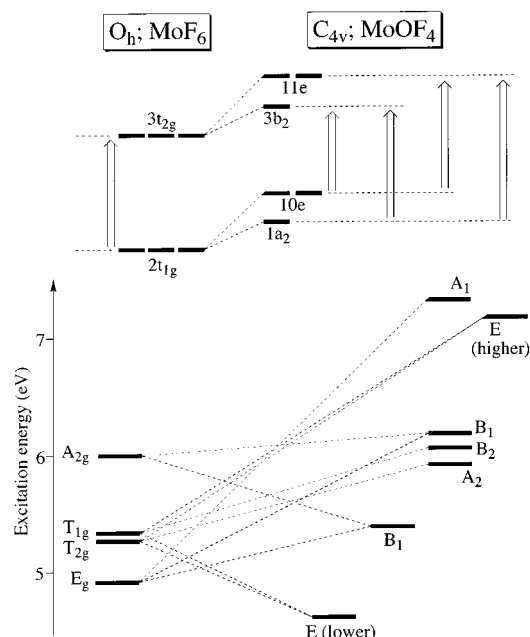
Figure 6. Comparison between the $2t_{1g} \rightarrow 3t_{2g}$ excitation of the MoF_6 and the corresponding excitation of $MoOF_4$. The excitation energies are calculated by the SAC-CI method.
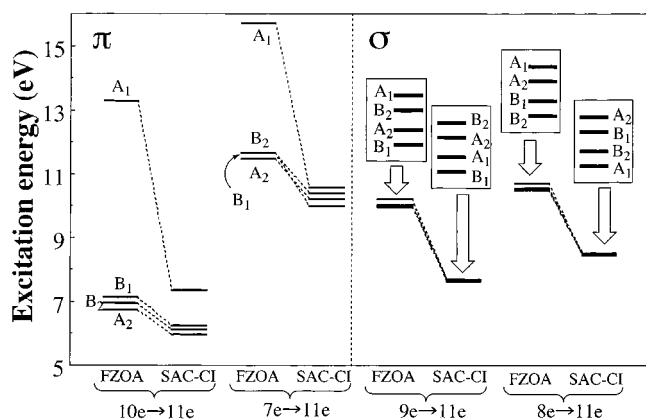

Figure 7. Comparison of the excitation energies of the $MoOF_4$ calculated by the FZOA and SAC-CI methods.

TABLE 8: MO Integrals Contributing to the Splittings and Intensities in the (10e, 7e, 8e, and 9e) $\rightarrow$ 11e Excitations of $MoOF_4$

	$^1A_1$, $^1B_1$			$^1A_2$, $^1B_2$		
main config.	K_{ia}	$(ai\lfloor jb)$	$\langle \Phi_i{}^a \vert r \vert 0 \rangle$	K_{ib}	$(bi\lfloor ja)$	$\langle \Phi_i{}^b \vert r \vert 0 \rangle$
π character						
$10e \rightarrow 11e$	2.2091	1.6301	1.6320	0.1460	0.1436	0.0
$7e \rightarrow 11e$	1.6818	1.0920	0.5259	0.1295	0.1260	0.0
σ character						
$8e \rightarrow 11e$	0.1272	0.0585	0.2039	0.0421	0.0091	0.0
$9e \rightarrow 11e$	0.1659	0.0532	0.1625	0.0433	0.0094	0.0

gaps belonging to the $9e \rightarrow 11e$ and $8e \rightarrow 11e$ excitations are only 0.075 and 0.071 eV, respectively.

As it has been already seen in MoF_6, the difference between K_{ia} and K_{ib} is dominant for the B term and that between $(ai\lfloor jb)$ and $(bi\lfloor ja)$ for the C term. The following relationships may be deduced from the data shown in Table 8: $K_{ia} > K_{ib}$, $(ai\lfloor jb) > (bi\lfloor ja)$, and $\langle \Phi_i{}^a \vert r \vert 0 \rangle > \langle \Phi_i{}^b \vert r \vert 0 \rangle$. Moreover, values of K_{ia} and $(ai\lfloor jb)$ integrals, for the $(8e, 9e) \rightarrow 11e$ excitations, are 1 order of magnitude smaller than those corresponding to the $(10e, 7e) \rightarrow 11e$ excitations. How these large energy differences of the exchange and four-index integrals come about is explained and
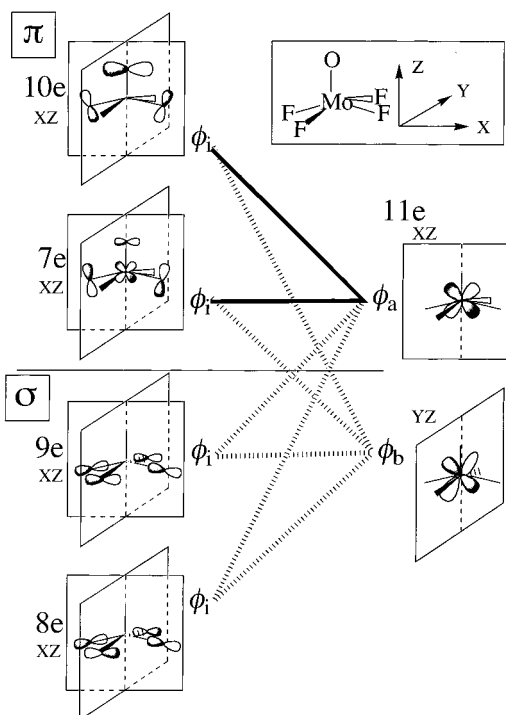
Figure 8. Combination of the orbitals of $MoOF_4$ for the transition density. The solid and dotted lines are large and small overlaps between them, respectively.

rationalized by using the transition density $\phi_a{}^*(r) \phi_i(r)$, as shown in section III.B for MoF_6.

Figure 8 shows schematic illustrations of the $\phi_a{}^*(r) \phi_i(r)$ and $\phi_b{}^*(r) \phi_j(r)$ orbital combinations for the (10e, 7e, 9e, and 8e) $\rightarrow$ 11e excitations. The (ϕ_a, ϕ_i) and (ϕ_b, ϕ_j) MO pairs, which are b_1 and b_2 symmetries in the C_{2v} subset, respectively, have maximum amplitudes on the xz- and yz-planes, respectively. Since $\phi_a(r)$ and $\phi_i(r)$ have a larger overlap than that of $\phi_b(r)$ and $\phi_i(r)$, K_{ia} and $(ai\lfloor jb)$ integrals are much greater than K_{ib} and $(bi\lfloor ja)$ integrals. Energy differences between the (10e, 7e) $\rightarrow$ 11e and (9e, 8e) $\rightarrow$ 11e excitations are explained by the bonding characters. Namely, since the 7e and 10e MOs have π character, the overlaps with the 11e MOs are $\pi-\pi$ types (i.e., large). On the other hand, the 8e and 9e MOs actually being two σ-type and two π-type Mo$-$F bonds, the overlaps with 11e MO are mixed σ-π types (i.e., small). Small overlaps of the mixed σ-π type have been also seen in MoF_6.

IV. Final Remarks and Summary

In this work, we have applied the SAC/SAC-CI method to study the electronic structures of MoF_6 and $MoOF_4$ in the ground and excited states. Electron correlations were found important for accurate descriptions of the ground and excited states. In contrast to the formal charge (+6) of Mo in these molecules, the Mo$-$ligand bonds are found to be much neutralized and to have large covalent characters in both the ground and excited states, owing to the back-donation from ligands to Mo. The ionic character of the Mo$-$ligand bonds is further relaxed by including the electron correlations. The ionicity of $MoOF_4$ is calculated to be greater than that of MoF_6. Electronic transitions of both molecules below 11 eV are all characterized as the electron-transfer excitations from ligands to Mo, which reduce the polarities of the Mo$-$F and Mo$-$O bonds.

In the present study, we assign five experimental UV peaks of MoF_6 and two of $MoOF_4$. Discrepancies between the experimental and theoretical excitation energies are, at worst,

0.35 and 0.27 eV, respectively. Since the calculated oscillator strengths are also in qualitative agreement with experiments, the present assignments are more reasonable and reliable than the previous ones.

We have further applied the FZOA method to examine and explain the energy orderings and splittings for the excited states having the same excitation nature. For MoF$_6$, we discuss the excitations from cubic to cubic degenerate MOs: namely, (2t$_{1g}$, 1t$_{2u}$, 6t$_{1u}$, and 2t$_{2g}$) $\rightarrow$ 3t$_{2g}$. For MoOF$_4$, the excitations from quadratic to quadratic degenerate MOs, e $\rightarrow$ e, are analyzed. In the excited states of the π-character MOs, the energy splittings arise from the energy differences between the exchange integrals K_{ia} and K_{ib} and between the $(ai|jb)$ and $(bi|ja)$ type integrals. The quite different magnitudes of them are discussed and closely analyzed by using the transition density $\phi_a^*(r) \, \phi_i(r)$ or the overlaps between the $\phi_a(r)$ and $\phi_i(r)$ MOs. The FZOA method, in this respect, is simple and very useful for understanding the chemical and physical terms of the meanings of the excitation levels. Some qualitative relationships established by the FZOA method may be suitable for any system. In particular, the following statement is believed to be valid for the singlet-excited states related with the π-character MOs:

"The dipole-allowed state is located at the highest energy level and is greatly split from the other states with the same excitation manifold nature."

References and Notes

(1) Karlsson, L.; Mattsson, L.; Jafrny, R.; Bergmark, T.; Siegbahn, K. *Phys. Scr.* **1976**, *14*, 230.

(2) Bloor, J. E.; Sherrod, R. E. *J. Am. Chem. Soc.* **1980**, *102*, 4333.

(3) Gutsev, G. L.; Boldyrev, A. I. *Mol. Phys.* **1984**, *53*, 23; *Chem. Phys. Lett.* **1983**, *101*, 441.

(4) Morita, H.; Nakai, H.; Tomasello, P.; Nakatsuji, H. *Bull. Chem. Soc. Jpn.* **1996**, *69*, 1893.

(5) Sakai, Y.; Miyoshi, E. *J. Chem. Phys.* **1987**, *87*, 2885. Miyoshi, E.; Sakai, Y.; Murakami, A.; Iwaki, H.; Terashima, H.; Shoda, T.; Kawaguchi, T. *J. Chem. Phys.* **1988**, *89*, 4193.

(6) McDiarmid, R. *J. Chem. Phys.* **1974**, *61*, 3333.

(7) Edwards, A. J.; Steventon, B. R. *J. Chem. Soc.* **1968**, *A1968*, 2503.

(8) Levason, W.; Narayanaswamy, R.; Ogden, J. S.; Rest, A. J.; Truff, J. W. *J. Chem. Soc., Dalton Trans.* **1981**, *1981*, 2501.

(9) Sosa, C.; Andzelm, J.; Elkin, B. C.; Wimmer, E.; Dobbs, K. D.; Dixon, D. A. *J. Phys. Chem.* **1992**, *96*, 6630.

(10) Neuhaus, A.; Veldkamp, A.; Frenking, G. *Inorg. Chem.* **1994**, *33*, 5278.

(11) Benson, M. T.; Cundari, T. R.; Lim, S. J.; Nguyen, H. D.; Pierce-Beaver, K. *J. Am. Chem. Soc.* **1994**, *116*, 3955.

(12) Nakatsuji H.; Hirao, K. *J. Chem. Phys.* **1978**, *68*, 2035.

(13) Nakatsuji, H. *Chem. Phys. Lett.* **1978**, *59*, 362; **1979**, *67*, 329, 334.

(14) Nakatsuji, H. *Acta Chim. Hung.* **1992**, *129*, 719. Nakatsuji, H. *Computational Chemistry Reviews of Recent Trends*; Leszczynski, J., Ed.; World Scientific: River Edge, NJ, 1997; Vol. 2.

(15) Nakai, H.; Morita, H.; Nakatsuji, H. *J. Phys. Chem.* **1996**, *100*, 15753.

(16) Seip, H. M.; Seip, R. *Acta Chem. Scand.* **1966**, *20*, 2698.

(17) Iijima, K. *Bull. Chem. Soc. Jpn.* **1977**, *50*, 373.

(18) Huzinaga, S.; Andzelm, J.; Klobukowski, M.; Radzio-Andzelm, E.; Sakai, Y.; Tatewaki, H. *Gaussian Basis Sets for Molecular Calculations*; Elsevier: New York, 1984.

(19) Jungen, M. *J. Chem. Phys.* **1981**, *74*, 750.

(20) Dunning, Jr., T. H.; Hay, P. J. *Modern Theoretical Chemistry*; Schaeffer, H. F., III, Ed.; Plenum: New York, 1977; Vol. 3.

(21) Dunning, T. H., Jr. *J. Chem. Phys.* **1970**, *53*, 2823.

(22) Dupuis, M.; Farazdel, A. Program System HONDO8 from MO-TECC-91, 1991.

(23) Nakatsuji, H. *Chem. Phys.* **1983**, *75*, 425.

(24) Nakatsuji, H. Program System for SAC and SAC-CI calculations, Program Library No. 146 (Y4/SAC), Data Processing Center of Kyoto University, 1985; Program Library SAC85, No. 1396, Computer Center of the Institute for Molecular Science, 1986.

(25) Hund, F. *Z. Phys.* **1925**, *33*, 345.